# Supplementary Material for 'Elucidating nanostructural organisation and photonic properties of butterfly wing scales using hyperspectral microscopy'

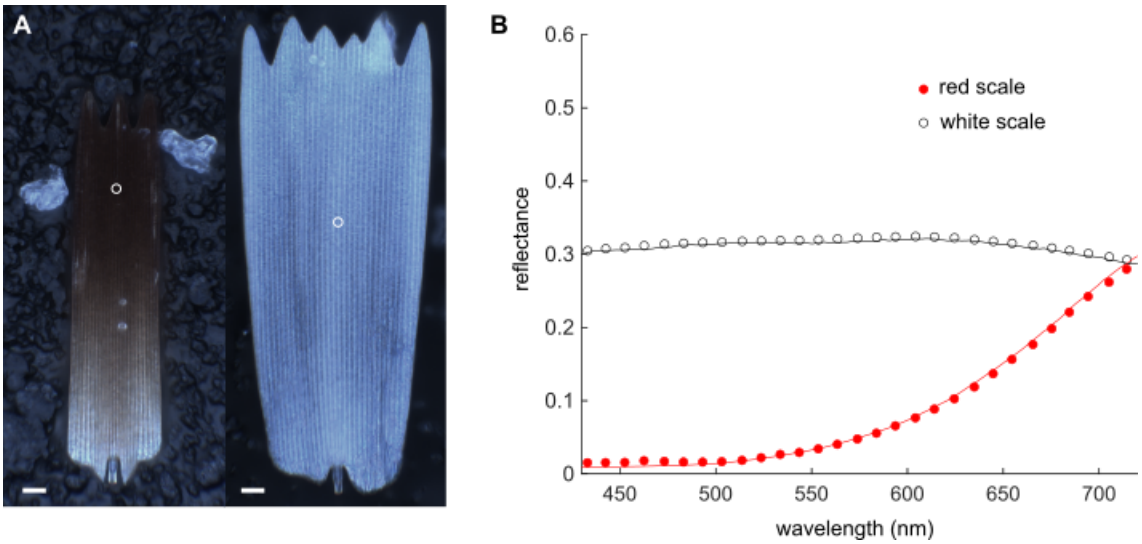


**Figure S1.** Reflectance spectra from small patches of a single red and white scale from the butterfly *Erora opisena* measured using hyperspectral microscopy (HSM) and microspectrophotometry (MSP). (A) Light microscopy images of single red (left panel) and white (right panel) wing scales taken with a 50× objective lens showing the locations of measurement areas producing the results shown in (B). (B) Reflectance spectra from each location in (A) measured using HSM (dots) and MSP (lines). The scale bars in (A) are 10 $\mu$m and the circles' sizes represent the measurement area for MSP.

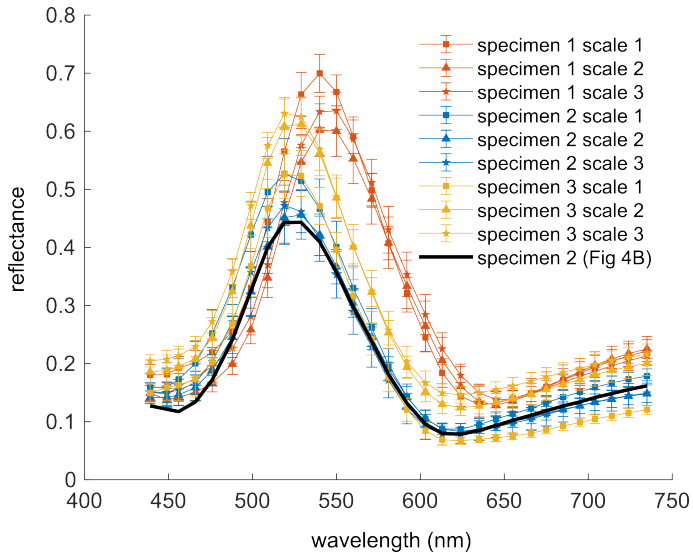


**Figure S2.** Reflectance spectra from the green wing scales of three *E. opisena* specimens. The relative reflectance of ten gyroid crystallites from three wing scales per specimen were measured and averaged using the 25 (NA = 0.8) objective lens. Measurements from each specimen are shown in a different colour (orange = specimen 1; blue = specimen 2; yellow = specimen 3) and different wing scales are represented by square, triangle, and star symbols. The solid black line shows data from Figure 4B that was collected from a different wing scale of specimen 2. This data was collected using a different reference measurement and hence has been scaled to approximately the same reflectance values of the other scales measured from the same specimen (specimen 2).

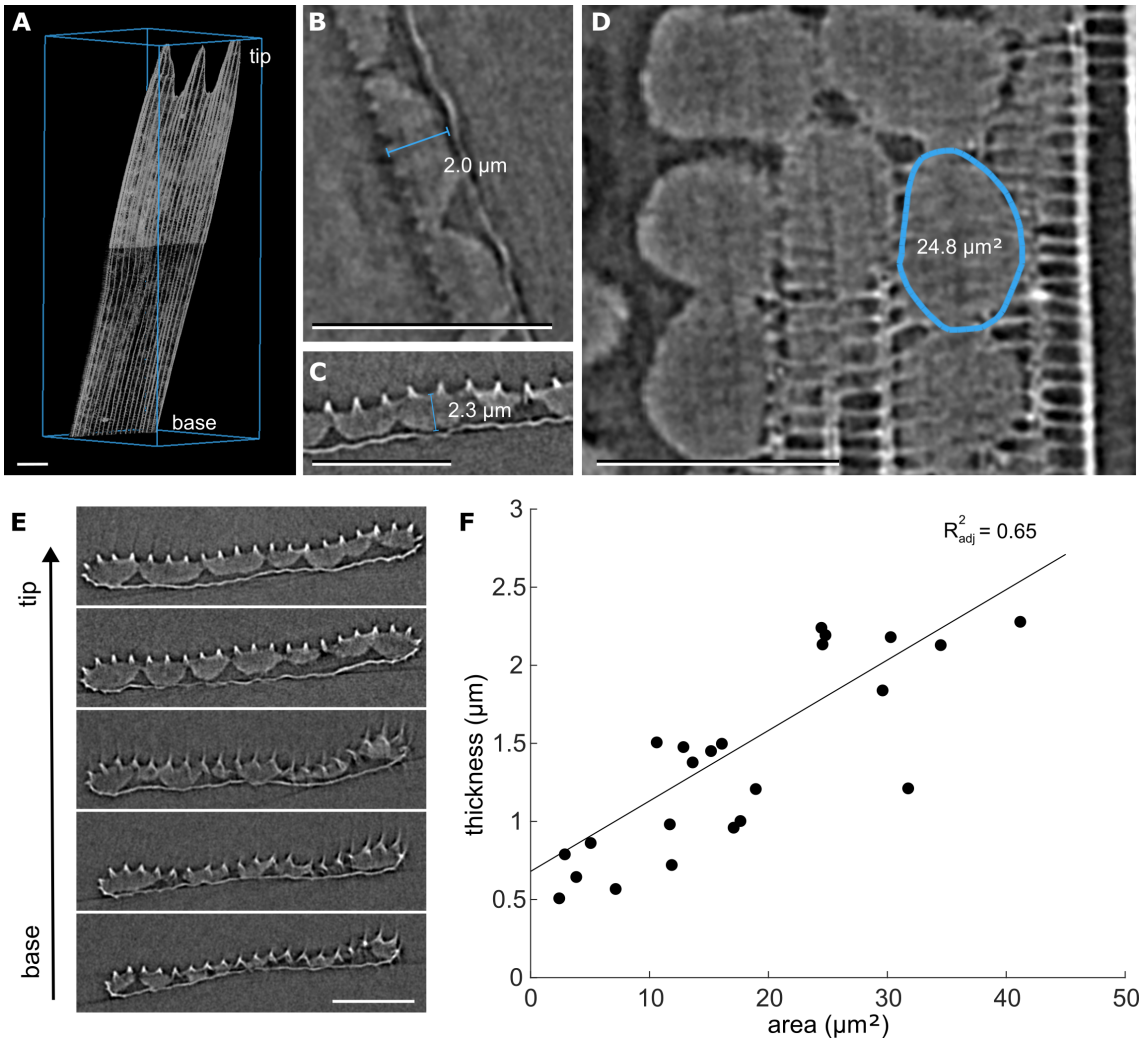


**Figure S3.** Reconstructed x-ray tomography data of a green wing scale from *E. opisena* that was used to measure the area and thickness of gyroid crystallites across the scale. (A) Three-dimensional reconstruction of the x-ray tomography data. (B, C, D) Slices through three different planes of the dataset showing cross-sections through a gyroid crystallite with corresponding thickness measurements taken from two different planes (B, C) and a cross-section along the scale showing a top-down view of the crystallite and the corresponding area measurement (D). (E) Slices along the scale from base to tip showing the variation in thickness of the crystallites from smallest at the base to largest at the tip. (F) Area versus average thickness (averaged over the two perpendicular cross-sectional planes) of gyroid crystallites showing that crystallites that cover a larger area (from a top-down view) are also thicker. The trend line is a linear regression line calculated using the linear least squares method, with an adjusted $R^2$ value of 65%.

**Table 1. Gyroid simulation parameters.** FDTD simulations were conducted on single gyroid structures with varying structural parameters as outlined in the table. Solid volume fraction = $\phi$, lattice parameter = $a$, nodal threshold = $t$, area = $A$, thickness = $T$, refractive index of chitin = $n^{\text{chitin}}$, refractive index of air = $n^{\text{air}}$. Simulations were conducted with PML boundary conditions on all boundaries except for the model varying the lattice parameter that had periodic boundary conditions

| Model | $\phi$ | $a$ | $t$ | $A$ | $T$ | $n^{\text{solid}}$ | $n^{\text{air}}$ |
|---|---|---|---|---|---|---|---|
| | [1] | $[nm]$ | [1] | $[\mu\text{m}^2]$ | $[\mu\text{m}]$ | $[\mu\text{m}]$ | $[\mu\text{m}]$ |
| Gyroid solid volume fraction | 0.8:0.15 | 330 | -0.91:1.06 | 15.68 | 1.00 | 1.56 | 1.00 |
| Gyroid lattice parameter | 0.30 | 250:400 | 0.62 | 15.68 | 1.00 | 1.56 | 1.00 |
| Gyroid thickness | 0.30 | 330 | 0.62 | 15.68 | 0.5:2.5 | 1.56 | 1.00 |

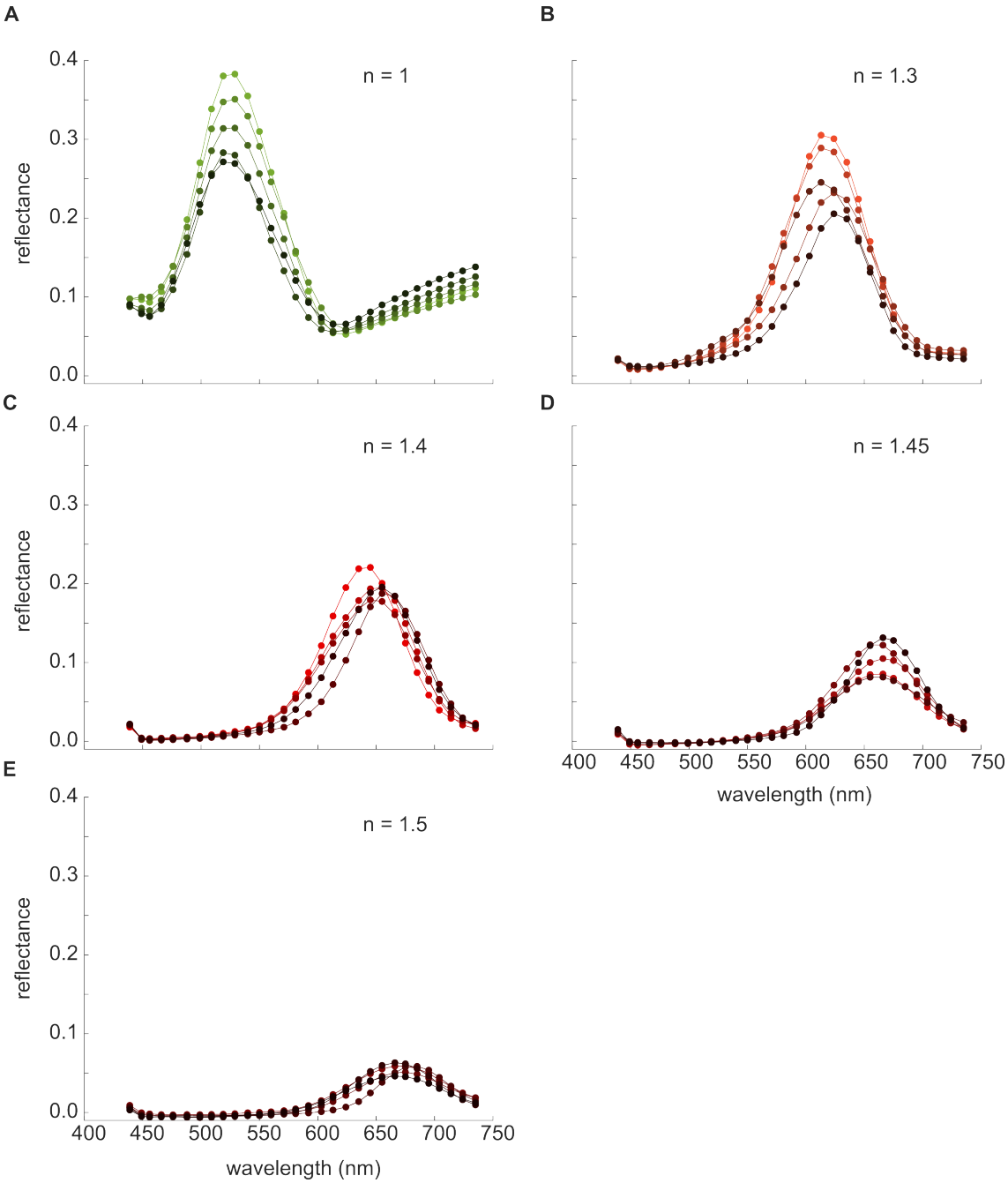


**Figure S4.** Raw data used to generate average reflectance curves in Fig. 5 of the main paper: Reflectance spectra from five different crystallites immersed in air and refractive index matching oils. These spectra represent the spectra corresponding to 5 of the 10 crystallites which were analysed in Fig. 5 of the main paper.

**Table 2. Multilayer simulation parameters.** FDTD simulations were conducted on multilayer structures with varying structural parameters as outlined in the table. All simulations included five layers except those where the number of layers was varied (yellow). In these simulations the period size was set to 0.2 and the solid volume fraction to 0.5. All simulations were conducted on layers of chitin ($n$=1.56) and air ($n$=1.0).

| Multilayer - varying volume fraction | | | | | | | | |
|---|---|---|---|---|---|---|---|---|
| Chitin layer thickness [$\mu$m] | 0.2 | 0.22 | 0.24 | 0.26 | 0.28 | 0.3 | 0.32 | 0.35 |
| Air layer thickness [$\mu$m] | 0.25 | 0.23 | 0.21 | 0.19 | 0.17 | 0.15 | 0.13 | 0.1 |
| Periodicity [$\mu$m] | 0.45 | 0.45 | 0.45 | 0.45 | 0.45 | 0.45 | 0.45 | 0.45 |
| Solid volume fraction | 0.44 | 0.49 | 0.53 | 0.58 | 0.62 | 0.67 | 0.71 | 0.78 |
| **Multilayer - varying air layer thickness** | | | | | | | | |
| Chitin layer thickness [$\mu$m] | 0.225 | 0.225 | 0.225 | 0.225 | 0.225 | 0.225 | 0.225 | 0.225 |
| Air layer thickness [$\mu$m] | 0.1 | 0.12 | 0.14 | 0.18 | 0.225 | 0.25 | 0.275 | 0.29 |
| Periodicity [$\mu$m] | 0.325 | 0.345 | 0.365 | 0.405 | 0.45 | 0.475 | 0.5 | 0.515 |
| Solid volume fraction | 0.69 | 0.65 | 0.62 | 0.55 | 0.5 | 0.47 | 0.45 | 0.44 |
| **Multilayer - varying periodicity** | | | | | | | | |
| Chitin layer thickness [$\mu$m] | 0.09 | 0.1 | 0.12 | 0.13 | 0.14 | | | |
| Air layer thickness [$\mu$m] | 0.09 | 0.1 | 0.12 | 0.13 | 0.14 | | | |
| Periodicity [$\mu$m] | 0.18 | 0.22 | 0.24 | 0.26 | 0.28 | | | |
| Solid volume fraction | 0.5 | 0.5 | 0.5 | 0.5 | 0.5 | | | |

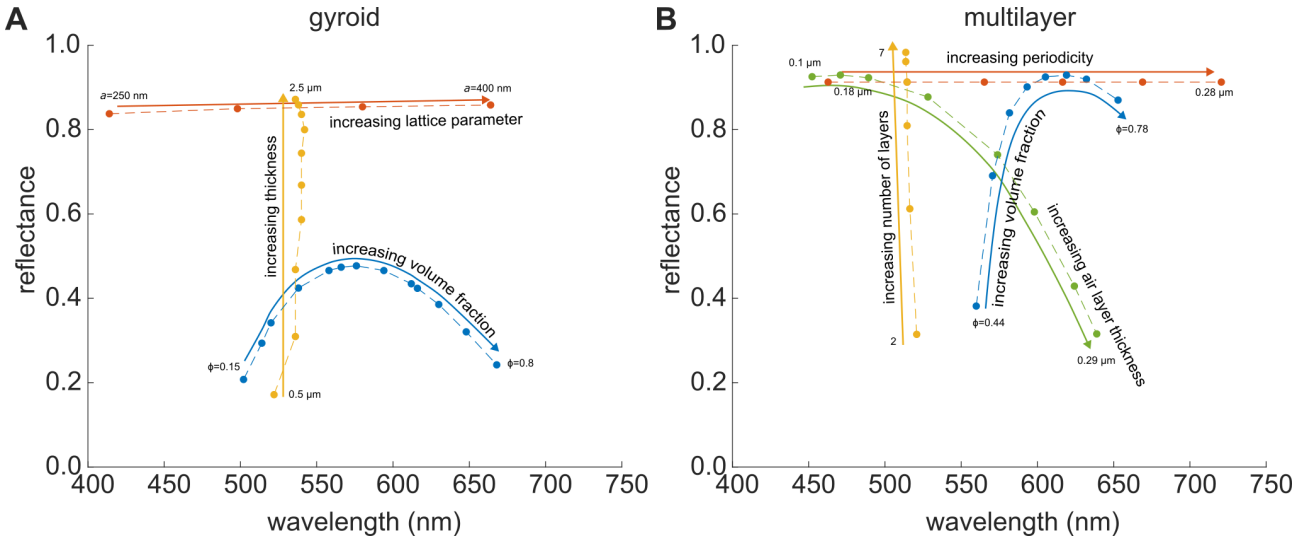


**Figure S5.** Variations of peak reflectance and peak wavelength (of the dominant peak) for several structural transition models of single gyroid and multilayer nanostructural geometries, as obtained by FDTD simulations. (A) The blue curve represents a chitin single gyroid structure in air where the volume fraction $\phi$ of the chitin phase is increased. The yellow curve is a thin film of increasing thickness which is internally structured by a single gyroid geometry of fixed size and volume fraction. The orange curve corresponds to an 'affinely scaled' gyroid geometry where, while maintaining fixed chitin volume fraction and number of unit cells, the lattice parameter is continuously increased. All gyroid geometries are aligned so that the [110] direction corresponds to the (vertical) direction of incident light. (B) Optical simulations of a multilayer structure where individual parameters are varied. The orange curve is an 'affinely scaled' multilayer where, at fixed relative volume fraction of the chitin and air layer, the spacing is increased. The yellow curve represents a multilayer stack where the number of layers is increased, while keeping layer thicknesses the same. The blue curve corresponds to a 'swelling' of the air phase, i.e. increasing the thickness of the air layer while keeping the chitin layer the same; the blue curve is a deformation that increases the thickness (or volume fraction) of the chitin layer while maintaining a constant spacing (i.e., at the expense of the air layer). The structural parameters for all transformations are described in Table 1 and 2. The behaviour of the curves at lower dielectric contrast (e.g., when air is replaced by water or cytosol or/and when chitin is replaced by a refractive index corresponding to a membrane) would be qualitatively similar, albeit with significantly lower reflectance values and spectral shift.

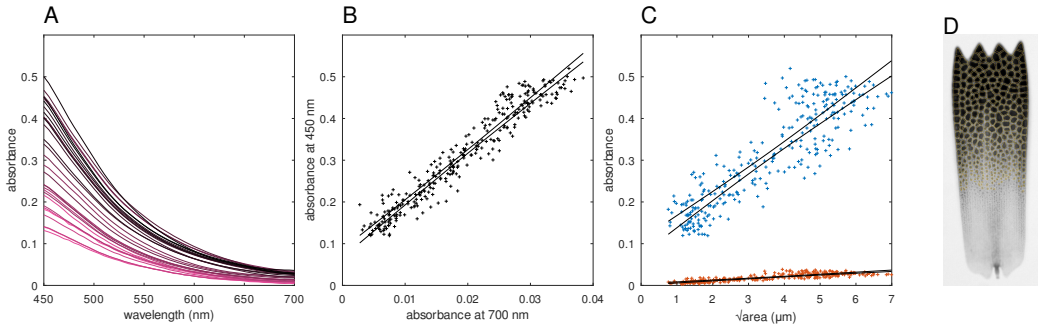


**Figure S6.** Analysis of pigmentary absorbance in wing scales by immersion in index-matched oil which 'neutralises' the photonic crystal nanostructure and minimises scattering. The scale was immersed in oil with n=1.55 and covered with a coverslip. The transmitted light aperture diaphragm was left open, NA=0.90. Hyperspectral image series was taken with the 50x (NA=0.95) objective. **(A)** A subset of absorbance spectra of 300 individual crystallites. Larger crystallites (*black*) tend to have higher absorbance than smaller crystallites (*magenta*). The largest crystallites block up to $\approx 70\%$ of the large aperture incident light cone at 450nm. The blockage appeared even stronger when a small aperture illumination cone (NA $\leq 0.3$) was used (*not shown*). **(B)** Regression between the measured absorbance at 700 nm and 450 nm. Linear regression using model $A_{450}(A_{700}) = \alpha_0 + \alpha_1 A_{700}$ estimated the coefficients $(\pm SE)$ to $\alpha_0 = 0.0771 \pm 0.0039, \alpha_1 = 12.20 \pm 0.186, r^2 = 0.936$. The lines (*black*) show the 99% confidence range of the model. The absorbance at 450 nm is about 12-fold higher than at 700 nm. The departure of the correlation from the origin ($\alpha_0 \neq 0$) hints that scattering was likely not completely eliminated. **(C)** Regression between the crystallite lateral dimension $d(\mu m)$, calculated as the square root of ROI area, and absorbance at 450 nm (*blue*) using model $A(d) = \alpha_0 + \alpha_1 d$ estimated the coefficients to be $\alpha_0 = 0.0916 \pm 0.0073, \alpha_1 = 0.0613 \pm 0.0018, r^2 = 0.787$. Regression with absorbance at 700 nm (*red*) yielded coefficient estimates $\alpha_0 = 0.00250 \pm 0.00066, \alpha_1 = 0.00466 \pm 0.00016, r^2 = 0.723$. This indicates that larger crystallites have a higher optical thickness. Assuming that the pigment is evenly distributed within the chitin phase, larger crystallites should be physically taller, supporting the morphological finding. Notwithstanding the possible scattering or other optical effects, extrapolation towards zero crystallite lateral dimension hints that there might be a minimal height for the smallest crystallites. **(D)** An image of the immersed scale, taken at 450 nm in transillumination. The overlay (*orange*) is showing the ROIs delineating individual crystallites that produced the analysed dataset.